



**HAL**  
open science

# Chemically activated high grade nanoporous carbons from low density renewable biomass (*Agave sisalana*) for the removal of pharmaceuticals

Ana Mestre, Fabian Hesse, Cristina Freire, Conchi O Ania, Ana Carvalho

## ► To cite this version:

Ana Mestre, Fabian Hesse, Cristina Freire, Conchi O Ania, Ana Carvalho. Chemically activated high grade nanoporous carbons from low density renewable biomass (*Agave sisalana*) for the removal of pharmaceuticals. *Journal of Colloid and Interface Science*, 2019, 536, pp.681-693. 10.1016/j.jcis.2018.10.081 . hal-02108468

**HAL Id: hal-02108468**

**<https://hal.science/hal-02108468>**

Submitted on 6 Nov 2020

**HAL** is a multi-disciplinary open access archive for the deposit and dissemination of scientific research documents, whether they are published or not. The documents may come from teaching and research institutions in France or abroad, or from public or private research centers.

L'archive ouverte pluridisciplinaire **HAL**, est destinée au dépôt et à la diffusion de documents scientifiques de niveau recherche, publiés ou non, émanant des établissements d'enseignement et de recherche français ou étrangers, des laboratoires publics ou privés.



27 **Abstract**

28 *Hypothesis*

29 Enlarging the range of viable nanoporous carbon precursors, namely by the acid  
30 treatment of low density biomass residues, can overcome issues related with the  
31 availability and quality of raw materials that have potential impact on cost and quality  
32 grade of the final product.

33 *Experiments*

34 Nanoporous carbons were prepared following a two-step process: H<sub>2</sub>SO<sub>4</sub>  
35 digestion/polycondensation of biomass waste (*Agave sisalana*, sisal) to obtain acid-  
36 chars that were further activated with KOH or K<sub>2</sub>CO<sub>3</sub>. Selected synthesized nanoporous  
37 carbons were tested for the removal of pharmaceutical compounds - ibuprofen and  
38 iopamidol - in aqueous solutions.

39 *Findings*

40 The structure and density of the acid-chars are highly dependent on the concentration of  
41 H<sub>2</sub>SO<sub>4</sub> used in the digestion and polycondensation steps. An adequate choice of the  
42 acid-char synthesis conditions, activating agent and contact method allowed to feature  
43 nanoporous carbons with specific surface areas ranging from 600 to 2300 m<sup>2</sup> g<sup>-1</sup> and  
44 apparent densities reaching 600 kg m<sup>-3</sup>. The adsorption capacity of a sample obtained by  
45 KOH-activation for the removal of micropollutants from water was twice higher than  
46 the value attained by golden activated carbon (Cabot-Norit) commercialized for this  
47 specific purpose.

48

49 **Keywords:** sisal; biomass thermochemical conversion; K<sub>2</sub>CO<sub>3</sub> and KOH activation;  
50 nanoporous carbons; nitrogen adsorption isotherms; kinetic assays; equilibrium  
51 adsorption data; pharmaceutical compounds removal, ibuprofen; iopamidol.

52

## 53        **1. Introduction**

54    The use of residues for the production of valuable products has become a common  
55    practice in several economic sectors, as it contributes to the implementation of a circular  
56    economic strategy adopted by European Union and aligned with United Nations 2030  
57    Agenda for Sustainable Development.

58    In the manufacture of activated carbons at industrial scale, the choice of the precursors  
59    is an important issue due to various aspects as price fluctuations, availability and  
60    variability of sources, that can compromise the quality and price of the final product.

61    Coconut-shell is a key precursor in the fabrication of activated carbons [1] due to its low  
62    ash content which leads to activated carbons with low metals percentage, very good  
63    attrition resistance and generally high surface areas [2, 3]. Coal and wood are also  
64    widely used precursors; however coal-derived materials usually have large ash contents,  
65    while wood-derived granular activated carbons display poor attrition resistance. Other  
66    renewable sources (*e.g.* fruit shells and stones) are also employed at industrial scale for  
67    the manufacture of activated carbons, with less expression. From an academic point of  
68    view, the list of precursors for the preparation of activated carbons is quite large, as  
69    shown in various reviews [4-8].

70    The search for alternative synthetic routes that allow the preparation of high grade  
71    activated carbons from biomass residues (particularly low density biomass), is an issue  
72    of academic and industrial relevance. The use of renewable feedstocks is expected to  
73    have important environmental and economic impacts, since it allows to close the loop of  
74    many biomass wastes through their use in the production of valuable tradeable goods.

75    Conventional activation methods usually starts either by the carbonization of the  
76    biomass - to remove volatile matter - and further thermal treatment of the char in the  
77    presence of an oxidizing agent to develop the pore network (physical activation); or by  
78    the activation of the precursor mixed with an activating agent (chemical activation) [2].

79 Besides porosity, the density and hardness of the activated carbons strongly depend on  
80 the properties of the precursor, with low density ones typically leading to low density  
81 and soft (low attrition resistance) carbons [9].

82 Alternative carbonization and activation approaches have been largely explored for the  
83 past decades aiming at reducing the energy consumption, while producing highly  
84 porous activated carbons with controlled pore architectures. Among them, the  
85 hydrothermal carbonization of polysaccharides followed by the activation of the  
86 hydrochar has emerged as an interesting method that allows the preparation of  
87 superactivated carbons [10-13] with microspherical morphology [12-14] and improved  
88 performance for various applications (e.g., energy storage/production, gas adsorption)  
89 [11, 14-16]. On the other hand, two of the main constituents of lignocellulosic biomass,  
90 *i.e.* cellulose and hemicellulose, are complex structures composed by saccharic units  
91 (pentoses and hexoses). Therefore, following a similar approach, it is possible to obtain  
92 a char after the acid digestion and polycondensation of biomass [17]. Such acid-char  
93 may be used as carbon rich precursor for the synthesis of activated carbons.

94 In this study, a series of high grade nanoporous carbons were prepared from the acid  
95 digestion and polycondensation of a biomass residue (*Agave sisalana*), and evaluated  
96 for the removal of emerging pollutants from aqueous solution (*i.e.* ibuprofen and  
97 iopamidol). The acid-chars obtained after the acid digestion and polycondensation of the  
98 biomass were chemically activated using KOH and K<sub>2</sub>CO<sub>3</sub>. The effect of the acid  
99 digestion conditions in the apparent density, porosity and composition of both the acid-  
100 chars and their corresponding nanoporous carbons after chemical activation was  
101 investigated. The resulting nanoporous carbons displayed moderate to high surface area  
102 with some samples outperforming a commercial benchmark carbon for the removal of  
103 pharmaceutical compounds – ibuprofen and iopamidol – from aqueous solution.

## 104 2. Experimental section

### 105 2.1 Synthesis of the acid-chars

106 Sisal (*Agave sisalana*) residues received from a rope industry (Cordex, Portugal) were  
107 used as raw precursor. This biomass is composed by (wt./wt.) 65.8% of cellulose,  
108 12.0% of hemicellulose, 9.9% of lignin, 0.8% of pectin, and 0.3% of wax and water  
109 soluble compounds [18]; therefore about 78% of its structure is constituted by saccharic  
110 units. The synthesis of the sisal-derived acid-chars was inspired in the work of Wang *et*  
111 *al.* [19] on other biomass precursor (*i.e.* rice husk). Briefly, sisal fibers of ca. 1 cm long  
112 were digested under stirring in H<sub>2</sub>SO<sub>4</sub> solutions (Sigma-Aldrich, 95-98%) for 15 min in  
113 the case of 12 and 13.5 M solutions, and for 30 min in the case of 9 M solutions. In all  
114 cases a 1:10 wt./v ratio (g of sisal to cm<sup>3</sup> of H<sub>2</sub>SO<sub>4</sub> solution) was used and the treatment  
115 was carried out at 50 °C, controlled by a water bath (VWR Scientific Model 1201).  
116 After the acid digestion, the solid residue (undigested sisal fibres) was removed, and the  
117 dark acidic liquor was then heated at 90 °C under reflux during 6 h, to allow the  
118 polycondensation reactions rendering a solid product (acid-char). The polycondensation  
119 was carried out using acid concentrations equal or lower than those used in the digestion  
120 step. With exception of the acid-char prepared with H<sub>2</sub>SO<sub>4</sub> 13.5 M in both digestion and  
121 polycondensation steps additional 5 cm<sup>3</sup> of acid (same concentration as in the digestion  
122 step) or water were added per gram of biomass used. The acid-char was recovered by  
123 filtration, washed with distilled water until neutral pH, dried at 100 °C overnight and  
124 crushed in order to get a fine powder (particles with dimensions < 0.297 mm). The sisal-  
125 derived acid-chars were labelled as SX/Y, where X and Y correspond to the H<sub>2</sub>SO<sub>4</sub>  
126 concentration (M) used in the digestion and the polycondensation step, respectively  
127 (*e.g.* S9/9).

128 *2.2 Chemical activation of the acid-chars*

129 The acid-chars were activated with KOH or K<sub>2</sub>CO<sub>3</sub>, using various contacting methods,  
130 acid-char:activating agent ratios and activation temperatures. Two methods were used to  
131 allow the contact between the acid-char and the chemical activating agent: physical  
132 mixing of both powders in a mortar, and solution impregnation. In the former, the  
133 activation was carried out by mixing 1 g of the acid-char with K<sub>2</sub>CO<sub>3</sub> (Aldrich, 99 %) or  
134 KOH (Panreac, 85 %) in a weight ratio of 1:3 (acid-char:activating agent). In the case of  
135 solution impregnation, the activating agent is dissolved in water, mixed with the acid-  
136 char and stirred for 2 h at room temperature; the suspension was then dried at 80 °C to  
137 allow the evaporation of the excess water and crushed before the carbonization. The  
138 activation was performed at 700 or 800 °C for 1 h in a horizontal furnace (Thermolyne,  
139 model 21100) under a N<sub>2</sub> flow of 5 cm<sup>3</sup> s<sup>-1</sup> and using a heating rate of 10 °C min<sup>-1</sup>. After  
140 cooling down to room temperature under N<sub>2</sub> flow, the materials were washed with  
141 distilled water until neutral pH, dried overnight at 100 °C, crushed to a fine powder  
142 (particles with dimensions < 0.297 mm).

143 Activated carbons were labelled after the corresponding acid-chars followed by the  
144 activating agent (C for K<sub>2</sub>CO<sub>3</sub>, and H for KOH) and its amount per gram of acid-char  
145 (in g). Unless otherwise stated, samples were prepared by physical mixture and  
146 activated at 800 °C. The activated carbons prepared by solution impregnation were  
147 labelled with (s). As an example, sample S13.5/13.5/C3(s) corresponds to the carbon  
148 prepared by activation of acid-char S13.5/13.5 at 800 °C using 3 g of K<sub>2</sub>CO<sub>3</sub> and  
149 solution impregnation.

150 *2.3 Characterization of the materials*

151 Apparent -tapped- densities of the carbons were determined through a methodology  
152 adapted from the literature for powdered materials with 90 % of particles with  
153 dimensions lower than 0.177 mm (80 mesh) [20-22]. Briefly, a graduated cylinder was  
154 filled with a known amount (typically 0.5 g) of the powdered carbon (Mettler Toledo  
155 AB204-S/FACT), tapped in a rubber pad for several minutes until no further settling  
156 was observed, and the volume was recorded. The densities presented correspond to the  
157 mean value of at least three assays. The apparent densities were determined on a dry  
158 basis according to equation (1).

$$159 \quad \text{density} = 1000 \times \frac{\text{weight of sample, in g}}{\text{volume of sample, in cm}^3} \times \frac{(100 - \% \text{ moisture})}{100} \quad \text{Eq. 1}$$

160 The morphology of selected samples was evaluated by Scanning Electron Microscopy  
161 (SEM) performed at a Zeiss Supra 55 VP apparatus using 5 kV as accelerating voltage.  
162 Scanning was performed in situ on a sample powder without coating. The crystallinity  
163 of selected samples was assessed by X-ray powder diffraction (XRD) data obtained in a  
164 Pan Analytical PW3050/60X'Pert PRO apparatus equipped with a X'Celerator detector  
165 and with automatic data acquisition (X'Pert Data Collector (v2.0b) software). The  
166 diffractograms were collected at room temperature using monochromatized CuK $\alpha$   
167 radiation as incident beam (40 kV-30 mA), the 2 $\theta$  range of 5° to 60° was scanned with a  
168 step size of 0.017° and a time per step of 0.6 s.

169 The chemical composition of selected acid-chars was obtained by elemental analysis  
170 (CHNSO) using LECO CHNS-932 and LECO VTF-900 (for direct oxygen  
171 quantification) automatic analysers. Data is expressed in dry basis since the samples  
172 were previously dried at 105 °C. Diffuse reflectance infrared Fourier transform (DRIFT)  
173 spectroscopy was recorded in a Nicolet Magna-IR560 spectrometer provided with a  
174 high sensitivity mercury cadmium telluride detector (MCT-A) that operates at cryogenic

175 temperature. Spectra were recorded on powder samples without KBr addition. Each  
176 spectrum was obtained from the accumulation of 256 scans, recording with a spectral  
177 resolution of  $2\text{ cm}^{-1}$  in the mid-IR ( $4000\text{-}650\text{ cm}^{-1}$ ) spectral range. The pH at the point  
178 of zero charge ( $\text{pH}_{\text{PZC}}$ ) of the samples was measured following the reverse mass titration  
179 method [23] and using a Symphony SP70P pH meter. The thermal analysis (Setaram  
180 Labsys) was carried out on ca. 10-25 mg of sample under a nitrogen flow rate of  $50\text{ cm}^3$   
181  $\text{min}^{-1}$ , a heating rate of  $15\text{ }^\circ\text{C min}^{-1}$  and up to a final temperature of  $900\text{ }^\circ\text{C}$ . The ash  
182 content was determined after exposure of the samples at  $600\text{ }^\circ\text{C}$  in air, until constant  
183 mass.

184 The porosity of the samples was characterized by equilibrium adsorption/desorption  
185 isotherms of  $\text{N}_2$  at  $-196\text{ }^\circ\text{C}$  and  $\text{CO}_2$  at  $0\text{ }^\circ\text{C}$  measured in volumetric analysers from  
186 Micromeritics (ASAP 2010 and Tristar 3000, respectively). The samples (60-100 mg)  
187 were previously outgassed at  $120\text{ }^\circ\text{C}$  for 17 h under vacuum (pressure  $< 10^{-2}\text{ Pa}$ ). Data  
188 from the  $\text{N}_2$  isotherms were used to estimate the apparent surface area,  $A_{\text{BET}}$ , by the  
189 Brunauer-Emmett-Teller (BET) method, following the IUPAC [24, 25] and ISO 9277  
190 [26] recommendations for the determination of this parameter in microporous solids.  
191 The relative pressure range for the determination of the BET area was selected  
192 according with two criteria: (i) positive line intersect of multipoint BET fitting ( $C > 0$ )  
193 and (ii) maximum  $p/p^0$  value limited to the pressure range where  $n_{\text{ads}}(1-p/p^0)$   
194 continuously increases with  $p/p^0$  [25]. The total pore volume,  $V_{\text{total}}$ , was assessed using  
195 the Gurvich rule [27], that is, the number of  $\text{N}_2$  moles adsorbed at relative pressure close  
196 to unity (*i.e.*  $p/p^0 = 0.975$ ) converted in total pore volume assuming that the pores are  
197 filled with the condensed  $\text{N}_2$  in the normal liquid state. The  $\alpha_s$  method was also applied  
198 to the  $\text{N}_2$  adsorption data, taking as reference the isotherm reported by Rodríguez-  
199 Reinoso *et al.* [28], enabling to quantify the total micropore volume,  $V_{\alpha\text{ total}}$ , and also the

200 ultra,  $V_{\alpha \text{ ultra}}$ , and supermicropore,  $V_{\alpha \text{ super}}$ , volumes. The total micropore volume (width  
201  $< 2.0$  nm) was obtained by back extrapolation of the  $\alpha_s$  plots linear region at high  
202 relative pressure ( $\alpha_s > 1$ ) while the ultramicropore volume (width  $< 0.7$  nm) was  
203 evaluated by the interception of the linear range defined by the experimental data  
204 between  $p/p^0$  of 0.02 and, about, 0.4. The supermicropore volume ( $0.7 < \text{width} < 2.0$   
205 nm) corresponds to the difference  $V_{\alpha \text{ total}} - V_{\alpha \text{ ultra}}$ . The microporosity was also quantified  
206 by applying the Dubinin-Radushkevich (DR) equation to the  $N_2$  and  $CO_2$  adsorption  
207 data ( $W_{0 N_2}$  and  $W_{0 CO_2}$ , respectively). The pore size distribution (PSD) analysis in the  
208 micro-mesopore range was calculated from the  $N_2$  adsorption data using the 2D-  
209 NLDFIT-HS model that assumes surface heterogeneity and slit geometry of pores in  
210 activated carbons [29]. The micropore size distributions (MPSD) were further assessed  
211 from  $CO_2$  adsorption data according to the method proposed by Pinto *et al.* [30] that is a  
212 variation of the DR equation which does not imposes constraints to the shape of the  
213 distribution.

#### 214 *2.4 Liquid phase adsorption assays*

215 Selected acid-char derived activated carbons were tested along with a commercial  
216 benchmark carbon for the removal of two pharmaceutical compounds (PhCs) -ibuprofen  
217 and iopamidol- from aqueous solution. The commercial activated carbon - Norit SAE  
218 Super (NS) - from Cabot is a powdered material specially developed for wastewater  
219 treatment. According to the general characteristics reported in the datasheet provided by  
220 the supplier, carbon NS has an apparent (tapped) density of  $425 \text{ kg m}^{-3}$ , ca. 97 % of the  
221 particles have sizes lower than  $150 \mu\text{m}$ , and displays a basic character. Ibuprofen  
222 (sodium salt, Sigma-Aldrich – Lot BCBC9914V) and iopamidol (Hovione - Lot  
223 163926HQ01324) solutions were prepared with ultra-pure water without pH

224 adjustment. The solutions have a pH value around 5. About 6 mg of activated carbon  
 225 and a given volume of ibuprofen or iopamidol solution were mixed in glass vials  
 226 maintained at 30 °C (water bath, Grant GD100 controller) and stirred at 700 rpm  
 227 (multipoint agitation plate Poly, Variomag). Samples were collected after the desired  
 228 contact time (see details in Table 1). After removing the activated carbon by filtration,  
 229 the amount of ibuprofen or iopamidol remaining in solution was determined by UV-vis  
 230 spectrophotometry (Genesys 10S) at the wavelength of maximum absorbance (ca. 221  
 231 and 242 nm for ibuprofen and iopamidol, respectively). The PhC uptake was calculated  
 232 using the equation:

$$233 \quad q_t = \frac{C_0 - C_t}{W} \times V \quad \text{Eq. 2}$$

234 where  $q_t$  is the amount ( $\text{mg g}^{-1}$ ) of PhC adsorbed at time  $t$ ,  $C_0$  is the initial and  $C_t$  is the  
 235 PhC concentration at time  $t$  ( $\text{mg dm}^{-3}$ ),  $V$  is the volume of PhC solution ( $\text{dm}^3$ ) and  $W$  is  
 236 the weight (g) of dried carbon.

237 Screening adsorption tests, as well as kinetic and equilibrium assays were performed in  
 238 the experimental conditions summarized in Table 1 (mass, contact time, initial  
 239 concentration, volume). Given data correspond to the average value obtained in three  
 240 independent assays. Kinetic data were fitted to the linear forms of the pseudo-first and  
 241 pseudo-second order kinetic models [31] while the equilibrium adsorption data were  
 242 analysed considering the non-linear equations of the Langmuir [32] and Freundlich [33]  
 243 isotherm models.

244 **Table 1.** Experimental conditions and activated carbons used in the screening, kinetic and  
 245 equilibrium adsorption assays for the removal ibuprofen and iopamidol.

| Assay | Activated carbons | Conditions    |                             |                                   | Contact time |
|-------|-------------------|---------------|-----------------------------|-----------------------------------|--------------|
|       |                   | $m_{AC}$ (mg) | $V_{PhC}$ ( $\text{cm}^3$ ) | $[PhC]_0$ ( $\text{mg dm}^{-3}$ ) |              |

|                          |  |   |         |           |               |
|--------------------------|--|---|---------|-----------|---------------|
| Screening                | S13.5/13.5/C3<br>S13.5/13.5/C3(s)<br>S13.5/13.5/H3(s)<br>S9/9/C3 | 6 | 30      | 180       | 18 h          |
| Kinetics                 | S13.5/13.5/C3(s)<br>S13.5/13.5/H3(s)<br>NS                       | 6 | 30      | 180       | 5 min to 24 h |
| Equilibrium<br>Isotherms | S13.5/13.5/C3(s)<br>S13.5/13.5/H3(s)<br>NS                       | 6 | 9 to 30 | 20 to 180 | 18 h          |

246

### 247 3. Results and discussion

#### 248 3.1 Characteristics of the acid-chars

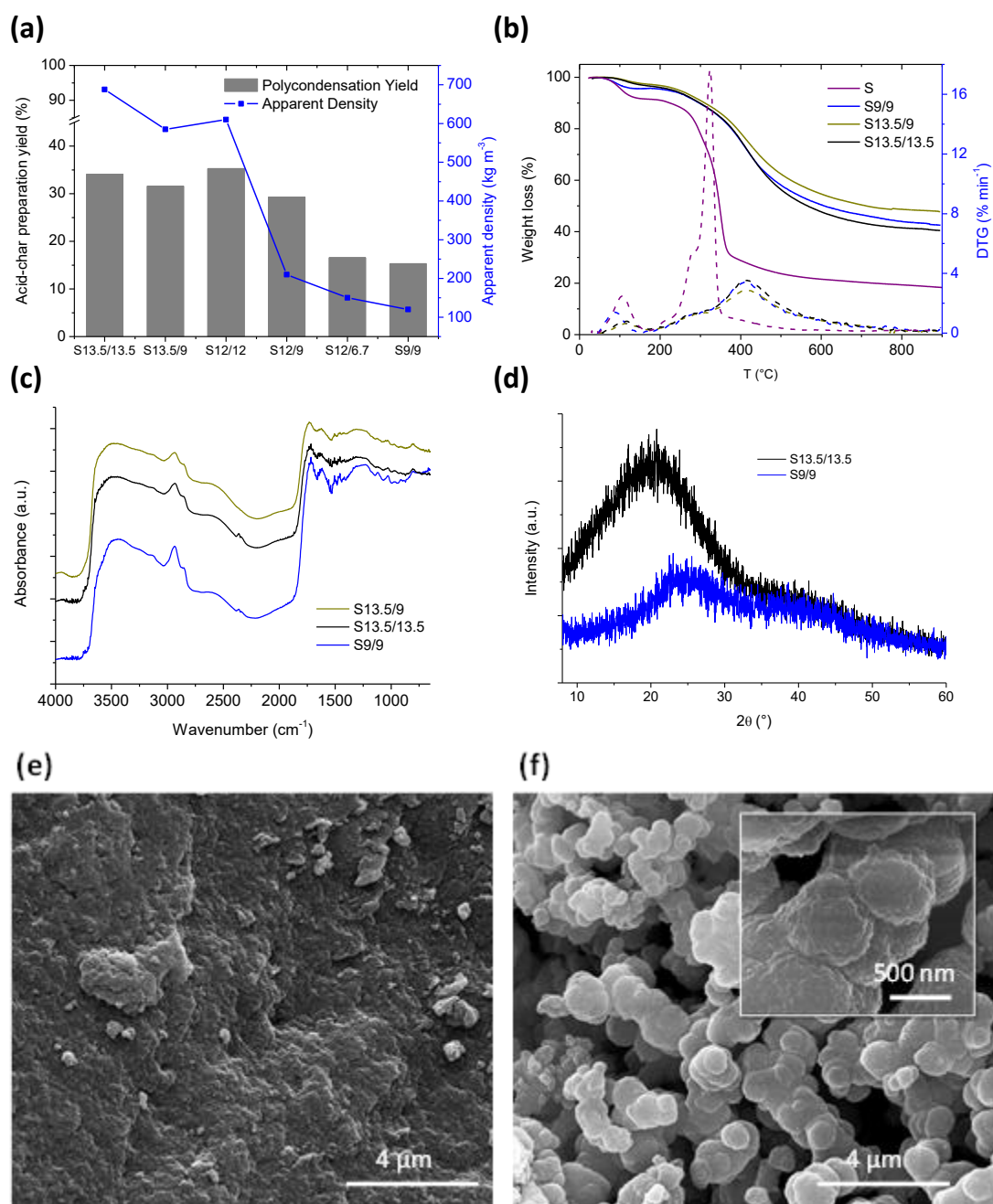
249 The use of different concentrations of H<sub>2</sub>SO<sub>4</sub> in the digestion and polycondensation  
 250 steps allowed to attain yields between 35-15 % (Figure 1(a)), being the highest value  
 251 slightly higher than that reported by Wang *et al.* [17] for rice husks in similar  
 252 experimental conditions. As seen, the concentration of sulphuric acid must be of at least  
 253 12 M in the digestion step, and 9 M in the polycondensation to reach yields above 30 %;  
 254 otherwise the yield dropped abruptly to 15 %. The elemental analysis data (Table S1)  
 255 confirmed the enrichment in carbon content and the decrease in the oxygen content of  
 256 the acid-chars, compared to the precursor. Despite the differences in the yields, the  
 257 composition of the acid-chars was quite similar (*i.e.*, 63 wt.% C, 4 wt.% H, 0.1 wt.% N,  
 258 0.23-0.41 wt.% S, and 32 wt.% O) and close to that of the rice husk-derived chars  
 259 reported in the literature using a similar procedure [19].

260 The use of different H<sub>2</sub>SO<sub>4</sub> concentrations seemed to have a small influence in the  
 261 thermal stability of the samples, as inferred from the thermogravimetric profiles (Figure  
 262 1(b)). The TG/DTG curves of the acid-chars present two weight loss steps: the first peak  
 263 appearing below 150 °C is attributed to moisture loss, while the second one between  
 264 200 and 800 °C corresponds to the main mass loss (ca. 50 %), linked to evolution of the

265 volatile matter remaining in the acid-chars. The pattern of the second peak features a  
266 shoulder at around 280 °C corresponding to the decomposition of labile (acidic) groups;  
267 the main loss at about 400 °C can be assigned to the decomposition of more stable  
268 oxygen containing functionalities and also some sulphur groups [34, 35]. These profiles  
269 are different from those of the pristine sisal fibres (S); the sharp peaks corresponding of  
270 the depolymerization of hemicelluloses, the cleavage of glucosidic linkages of cellulose  
271 and decomposition of cellulose oligomers into tars [18] are not observed in the acid-  
272 chars. This confirms the polycondensation of these monomers during the acid treatment  
273 at 90 °C.

274 Regarding surface chemistry, the DRIFT spectra of samples S13.5/13.5, S13.5/9 and  
275 S9/9 (Figure 1(c)) revealed similar profiles. The acid-chars present a broad band at  
276 3500-3200  $\text{cm}^{-1}$ , assigned to O-H stretching vibrations in surface hydroxylic groups [36,  
277 37]. The peaks  $\sim 2920 \text{ cm}^{-1}$  and  $\sim 2850 \text{ cm}^{-1}$  are assigned, respectively, to symmetric and  
278 asymmetric C-H stretching vibrations of aliphatic moieties of the acid-chars [36, 38].  
279 The peaks centred at 1755-1734  $\text{cm}^{-1}$  and 1637-1624  $\text{cm}^{-1}$  can be assigned to stretching  
280 vibrations of C=O moieties in various configurations (e.g., lactones, anhydrides, ester or  
281 carboxylic acid, and quinones) [36, 37]. The shoulder around 1580-1560  $\text{cm}^{-1}$  and the  
282 peak at 1510  $\text{cm}^{-1}$  are assigned to aromatic ring C=C stretching; this peak is red-shifted  
283 likely due to the high density of oxygen in the materials ( $\sim 32 \%$ , Table S1) [37]. The  
284 presence of aromatic ring C=C bonds points out the increase in the aromatization degree  
285 after the acid treatment. The peak at 1473-1454  $\text{cm}^{-1}$  can be attributed to carboxyl-  
286 carbonate structures [36, 37], and the band around 1250  $\text{cm}^{-1}$  to ether structures (ether  
287 bridges between rings and C-O stretch in ether moieties) [37]. The peak at 955  $\text{cm}^{-1}$  can  
288 also be assigned to C-O-C vibrations in cyclic anhydrides [37], while bands below 950

289  $\text{cm}^{-1}$  (i.e.  $905 \text{ cm}^{-1}$  and  $802 \text{ cm}^{-1}$ ) are characteristic of out-of-plane deformation  
290 vibrations of C-H groups in aromatic structures [36].



291

292

293 **Figure 1.** (a) Effect of  $\text{H}_2\text{SO}_4$  concentration in the digestion and polycondensation steps on the  
294 yields and tapped densities of the acid-chars; (b) thermogravimetric profiles (TG) and derivative  
295 (DTG) curves of selected samples; (c) DRIFT spectra and (d) XRD patterns of selected acid-  
296 chars. SEM images of samples (e) S13.5/13.5 and (f) S9/9 (a colour version of this figure can be  
297 viewed online).

298 Infrared spectra also revealed the presence of sulphur moieties, in agreement with the  
299 sulphur content detected by elemental analysis. The band at  $1119\text{ cm}^{-1}$  is assigned to  
300 stretching vibration in  $-\text{SO}_3\text{H}$  and the one between  $1034\text{-}1028\text{ cm}^{-1}$  to  $\text{S}=\text{O}$  stretching  
301 vibration. Both were more clearly observed in acid-char S9/9, and would contribute to  
302 the acidic nature of the acid-chars [38].

303 The acidic nature of the chars was confirmed by the low values of the  $\text{pH}_{\text{PZC}}$  (about 2  
304 pH units), regardless the  $\text{H}_2\text{SO}_4$  concentration used in the synthesis (Table S1). It should  
305 be highlighted that the presence of acidic oxygen groups is an important feature when  
306 envisaging further activation, as it is usually linked to a higher reactivity of the chars [6,  
307 39]. Additionally, it will allow a good dispersion and wettability of the materials in  
308 water, favouring the contact with the activating agent in the case of solution  
309 impregnation; this will be further discussed below.

310 According with the XRD patterns the acid-chars have an amorphous-like carbon  
311 structure, as evidenced by the broad and low-intensity diffraction peaks (Figure 1(d)).

312 The concentration of sulphuric acid has a low impact on the crystallinity of the samples,  
313 although, the samples prepared with the lower concentrations of acid presented lower  
314 structural order: (002) plane of graphite-like structures at ca.  $20^\circ$  for S13.5/13.5 while  
315 at ca.  $24^\circ$  and with lower intensity for S9/9. The diffraction peak at  $40^\circ$  is attributed to  
316 (101) crystalline planes of graphite in the microcrystalline regions of the carbon matrix.

317 The shift of both peaks compared to the values of graphite (ca.  $\sim 27^\circ$  (002) and  $\sim 45^\circ$   
318 (101) ICDD 25-284 [40]) is indicative of increased distance between crystalline plans.

319 This could be due to the presence of oxygen and sulphur groups, as evidenced by  
320 elemental analysis, DRIFT spectra data, and acidic  $\text{pH}_{\text{PZC}}$  values of these samples  
321 (Table S1).

322 On the other hand, the concentration of sulfuric acid had a dramatic influence on  
323 synthesis yields, the morphology and apparent densities. In fact, digestion in H<sub>2</sub>SO<sub>4</sub>  
324 13.5 M rendered high density acid-chars, regardless the concentration of acid used in  
325 the polycondensation step. In contrast, the density of the samples digested in H<sub>2</sub>SO<sub>4</sub>  
326 12 M was found to follow a different trend with the concentration of acid used in the  
327 polycondensation step. High density materials were obtained when the  
328 polycondensation was carried out in H<sub>2</sub>SO<sub>4</sub> 12 M, with the density decreasing sharply  
329 for lower concentration of sulfuric acid (from 600 to 150 kg m<sup>-3</sup>, Figure 1(a)). This  
330 behavior is certainly related with the morphological changes observed by SEM analysis  
331 (Figure 1(e) and (f)). While sample S13.5/13.5 has a compact morphology formed of  
332 small primary particles fused onto a dense and rough material, sample S9/9 is composed  
333 of interconnected spheres with diameters of around 500 nm, that originate an aerogel-  
334 like structure with an extended pore transport systems.

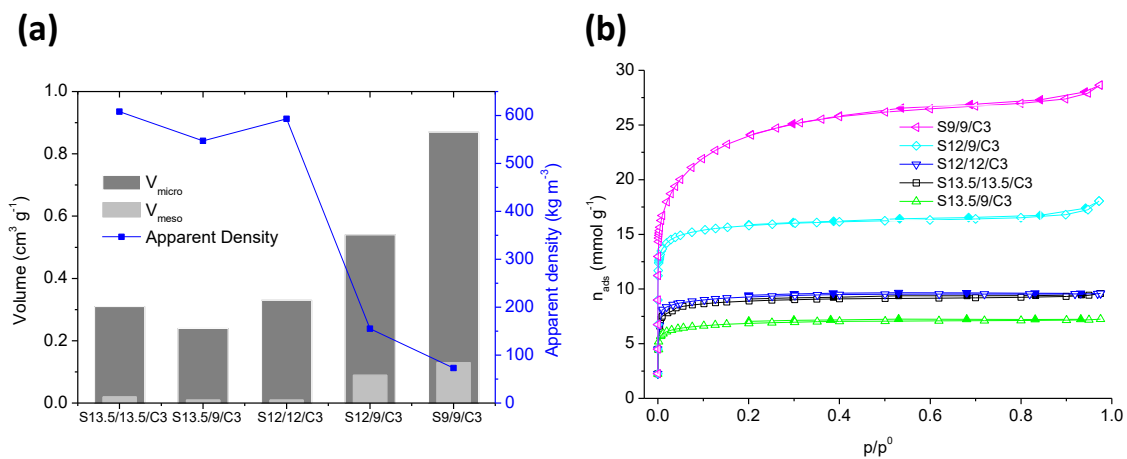
335 Summarizing, the selection of the concentration of H<sub>2</sub>SO<sub>4</sub> in both digestion and  
336 polycondensation steps controls the density of the acid-char, especially for values lower  
337 than 12 M. The higher yields obtained for the synthesis carried out in 12 M (or higher)  
338 H<sub>2</sub>SO<sub>4</sub> in both steps are related with a more effective extraction of the precursor's  
339 saccharic units, and a more extensive polycondensation reaction.

340 The N<sub>2</sub> adsorption data shows that the concentration of the acid does not influence the  
341 porosity of the acid-chars. All of them displayed type II isotherms (not shown)  
342 characteristic of materials with an incipient porosity [24]; accordingly, low surface area  
343 values (< 10 m<sup>2</sup> g<sup>-1</sup>) were obtained for all the acid-chars. However, important  
344 differences were observed in the porosity of the nanoporous carbons obtained after  
345 activation of the acid-chars (see discussion below).

### 346 *3.2 Characteristics of the nanoporous carbons*

347 The textural properties and apparent densities of the nanoporous carbons prepared by  
 348 activation of the acid-chars are clearly dependent on the  $\text{H}_2\text{SO}_4$  concentrations used in  
 349 the synthesis of the latter. Figure 2(a) shows the trends corresponding to samples  
 350 prepared by activation using  $\text{K}_2\text{CO}_3$  at 800 °C of various acid-chars.

351 As seen in Figure 2(b) all the carbons displayed type I isotherms according to the  
 352 IUPAC classification [24], indicating that they are essentially microporous materials.  
 353 Despite the similarities in chemical composition and stability of the acid-chars (Table  
 354 S1 and Figure 1(b)), large differences are observed in the porosity of the resulting  
 355 activated carbons. Carbons prepared by activation of low density acid-chars S9/9 and  
 356 S12/9 ( $< 200 \text{ kg m}^{-3}$ ) present at least twice the total pore volume of those prepared from  
 357 high density acid-chars ( $> 500 \text{ kg m}^{-3}$ ). Their pore network is composed by micropores  
 358 and about 13 % of mesopores. On the contrary, activated carbons S12/12/C3,  
 359 S13.5/9/C3 and S13.5/13.5/C3 are predominantly microporous samples.



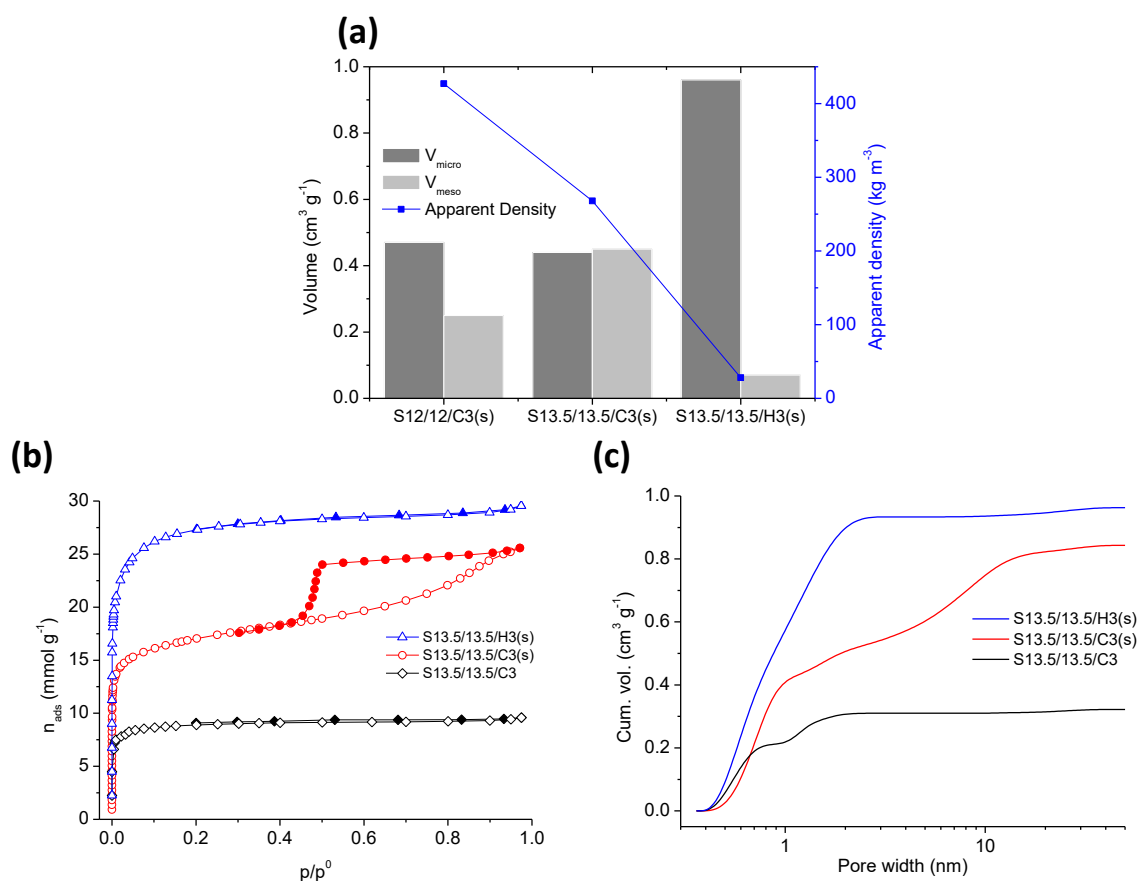
360 **Figure 2.** Properties of the activated carbons prepared by physical mixing with  $\text{K}_2\text{CO}_3$  (3 g  
 361  $\text{K}_2\text{CO}_3$  per gram of acid-char) followed by activation at 800 °C during 1 h (a) micro and  
 362 mesopore volumes and the influence of acid-char precursor in apparent density of the activated  
 363 carbons is also displayed, (b)  $\text{N}_2$  adsorption isotherms (a colour version of this figure can be  
 364 viewed online).

365 To evaluate the effect of the contact method between the precursor and the activating  
 366 agent, two samples S12/12 and S13.5/13.5 were prepared by activation using  $\text{K}_2\text{CO}_3$  by

367 physical mixture and solution impregnation (series s). Whereas physical mixing  
368 rendered carbons with a moderate porosity development, impregnation from solution  
369 allowed the preparation of micro-/mesoporous solids, with mesopore volumes  
370 accounting for ca. 50 % of the total pore volume (Fig. 3(b) and Fig. S1). The isotherms  
371 of the carbons obtained from solution impregnation present H2(a) type hysteresis loops  
372 [24, 41], indicating complex pore structures; the desorption branch of the hysteresis  
373 loop of carbon S13.5/13.5/C3(s) is steeper than the adsorption branch, pointing out to  
374 ink-bottle shape pores and pore-blocking effects. The relative pressure of the closing  
375 end of the hysteresis loop suggests cavitation-induced evaporation effects, characteristic  
376 of samples with narrow pore necks connecting the main mesopore cavities [24, 41].

377 It should be pointed out that this methodology (activation of acid-chars) allowed to  
378 prepare carbons with different textural features than those obtained by chemical  
379 activation of sisal wastes-themselves [42]. These are mainly microporous carbons [42,  
380 43] while herein described materials displayed a higher porosity development in the full  
381 micro-mesopore range, despite presenting similar global preparation yields (ca. 16-18 %  
382 for two-step and 17 % for optimized direct activation [44]).

383 Regarding the effect of the activating agent, the material obtained by KOH solution  
384 impregnation displayed the highest total pore volume, and a mainly micropore network  
385 as inferred from the shape of the nitrogen adsorption isotherm (type I and absence of  
386 hysteresis loop). The analysis of the pore size distribution obtained by applying the 2D-  
387 NLDFT-HS method to the N<sub>2</sub> adsorption data (Fig. 3(c)) confirms the dependence of  
388 the pore network characteristics with the contacting method and the activating agent.  
389 Physical mixing with K<sub>2</sub>CO<sub>3</sub> and solution impregnation with KOH rendered mainly  
390 microporous carbons, whereas the carbons prepared upon solution impregnation with  
391 K<sub>2</sub>CO<sub>3</sub> present a well-developed mesopore structure centered at about 7 nm.



392 **Figure 3.** (a) Micro and mesopore volumes of the activated carbons prepared by solution  
 393 impregnation of acid-chars S12/12 and S13.5/13.5 with K<sub>2</sub>CO<sub>3</sub> or KOH (3 g activating agent per  
 394 gram of acid-char) followed by activation at 800 °C during 1 h. The influence of acid-char  
 395 precursor in apparent density of the activated carbon is also displayed; (b) N<sub>2</sub> adsorption  
 396 isotherms of activated carbons prepared from acid-char S13.5/13.5; (c) Cumulative pore size  
 397 distributions obtained from the 2D-NLDFT-HS method applied to the N<sub>2</sub> adsorption isotherms  
 398 (A colour version of this figure can be viewed online).

399

400 Regarding morphology, images in Fig. S2 reveal that the roughness of the acid-char  
 401 S13.5/13.5 particles changed after activation, leading to particles with smooth and  
 402 exfoliated sections certainly due to the matrix consumption during activation (activation  
 403 yields around 50 %, Table 2). The XRD patterns of the activated materials (Fig. S3)  
 404 reveal the expected patterns of amorphous carbons with a low structural order.  
 405 Compared to the acid-chars the XRD patterns of the nanoporous carbons present  
 406 slightly more intense peaks at 2θ values of ca. 25 and 44°, corresponding to the  
 407 reflections of carbonaceous materials. This is associated to an increase in the

408 aromatization during the activation, and a low surface functionalization. In fact, both  
409 thermogravimetric analysis and infrared spectroscopy (Fig. S4) indicate that activation  
410 leads to a decrease in the surface functionalization (mass loss of *ca.* 15 wt.% for the  
411 activated carbon, compared to 56 wt.% for acid-char). Also  $\text{pH}_{\text{PZC}}$  values of samples  
412 S13.5/13.5/C3(s) and S13.5/13.5/H3(s) are less acidic than that of pristine acid-char  
413 (respectively, 3.8 and 4.9 versus 1.7).

414 Figure 4 shows smooth surfaces for the carbons obtained by  $\text{K}_2\text{CO}_3$  activation using  
415 physical mixing of high density acid-chars (samples S13.5/13.5, S13.5/9 and S12/12).  
416 For the low density acid-char (sample S9/9), the activation has less effect on the  
417 morphology (Figure 4). SEM images show that the impregnation in solution with  
418  $\text{K}_2\text{CO}_3$  seems to originate less compact particles; this is in line with the 50 % decrease  
419 in the density in sample S13.5/13.5/C3(s) compared to S13.5/13.5/C3 (Fig. 2(a) and  
420 3(a)), despite their similar activation yields (51 *versus* 45 %, Table 2). Activation with  
421 KOH leads to a pronounced morphological change, originating sponge-like particles  
422 that justify the very low apparent density of the final material ( $< 50 \text{ kg m}^{-3}$ ). Major  
423 morphology changes upon KOH activation of chars have also been reported in the  
424 literature [13, 14, 45], and can be justified by the distinct activation mechanisms  
425 between  $\text{K}_2\text{CO}_3$  and KOH. The KOH activation reactions start at 400 °C and lead to the  
426 formation of gases and K-compounds, which together activate the precursor; at  
427 converse, the decomposition of  $\text{K}_2\text{CO}_3$  starts at 700-800 °C, allowing a less extensive  
428 consumption of the matrix [46]. This fact also justifies the lower activation and global  
429 yields obtained upon KOH activation (Table 2).

430 The main textural parameters obtained from the analysis of  $\text{N}_2$  isotherms at -196 °C of  
431 the nanoporous carbons are compiled in Table 2. With exception of sample S9/9/C3, all  
432 the synthesized carbons present a wide distribution of micropores. By means of KOH

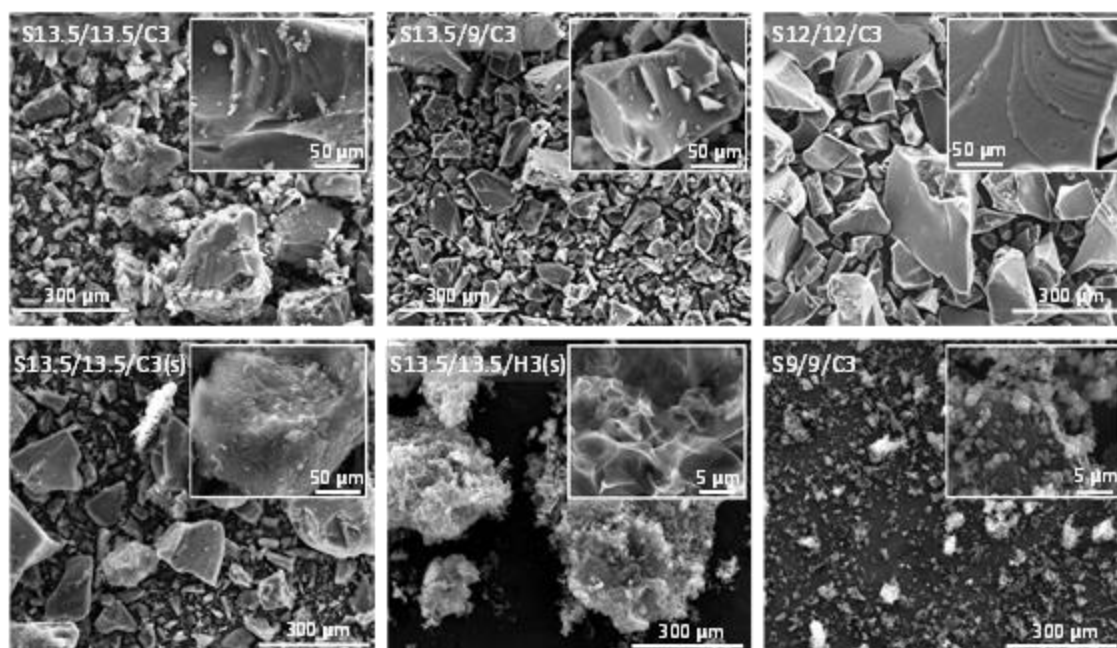
433 activation of high density acid-chars, or  $K_2CO_3$  activation of low density acid-chars, it is  
434 possible to attain surface areas higher than  $1900 \text{ m}^2 \text{ g}^{-1}$  and total pore volumes of  
435  $1.0 \text{ cm}^3 \text{ g}^{-1}$ . Such carbons are mainly composed of supermicropores; this is likely  
436 associated to the low activation and global yields (ca. 20 % and 3 %, respectively) and  
437 the low densities ( $< 100 \text{ kg m}^{-3}$ ).

438 The activation with KOH at  $700 \text{ }^\circ\text{C}$  allows higher yields but lower supermicropore  
439 volumes and still low density carbons. Compared to the carbons prepared by physical  
440 mixing, higher pore volumes and a well-developed network of mesopores are obtained  
441 upon solution impregnation with  $K_2CO_3$ . Furthermore, the activation and global yields  
442 are similar in both methods, pointing out that solution impregnation allows a more  
443 uniform and deeper penetration of the activating agent on the particles.

444 The microporosity was further analysed through  $CO_2$  adsorption isotherms. The  
445 micropore size distributions presented in Figure 5 reveal that the carbons prepared by  
446 physical mixing of high density acid-chars with  $K_2CO_3$  have narrow micropore  
447 distributions in the ultramicropore range, thus showing molecular sieve properties. The  
448 carbons prepared by solution impregnation with  $K_2CO_3$  or KOH present monomodal  
449 and continuous distributions in the range from 0.4 to 2.0 nm. Additionally, sample  
450 S9/9/C3 have bimodal distribution of micropores. It is important to note that the  
451 commercial carbon used as benchmark for the liquid adsorption assays also presented a  
452 bimodal distribution of micropores.

453 Interestingly, the surface area values follow an inverse correlation with the apparent  
454 densities of the nanoporous carbons; this allows to identity three major groups of  
455 samples linked with the properties of the acid-char, the contacting methodology and the  
456 activating agent. As seen in Figure 6, a fine control of the synthesis parameters allows

457 to prepare low density superactivated carbons ( $> 1800 \text{ m}^2 \text{ g}^{-1}$ ) and high density  
 458 materials with surface areas close to  $800 \text{ m}^2 \text{ g}^{-1}$ .



459

460 **Figure 4.** SEM images of the nanoporous carbons. The insets correspond to higher  
 461 amplifications to better illustrate the surface of the materials.

462

463 **Table 2.** Textural properties of the nanoporous carbons, activation and global yields.

| Sample               | Yield             |               | $A_{\text{BET}}$<br>( $\text{m}^2 \text{ g}^{-1}$ ) | $V_{\text{total}}^{\text{c}}$<br>( $\text{cm}^3 \text{ g}^{-1}$ ) | $V_{\text{meso}}^{\text{d}}$<br>( $\text{cm}^3 \text{ g}^{-1}$ ) | $\alpha_s$ Method   |   |   | DR Method   |  |
|----------------------|-------------------|---------------|---|---|--|---|---|---|---|--|
|                      | Activation<br>(%) | Global<br>(%) |   |   |  | $V_{\alpha}^{\text{total}}$<br>( $\text{cm}^3 \text{ g}^{-1}$ ) | $V_{\alpha}^{\text{ultra}}$<br>( $\text{cm}^3 \text{ g}^{-1}$ ) | $V_{\alpha}^{\text{super}}$<br>( $\text{cm}^3 \text{ g}^{-1}$ ) | $W_{\text{DR N}_2}$<br>( $\text{cm}^3 \text{ g}^{-1}$ ) | $W_{\text{DR CO}_2}$<br>( $\text{cm}^3 \text{ g}^{-1}$ ) |
| S13.5/13.5/C3        | 45                | 15            | 781   | 0.33  | 0.02   | 0.31  | 0.10  | 0.21  | 0.32  | 0.34   |
| S13.3/13.5/C3(s)     | 51                | 18            | 1419  | 0.89  | 0.45   | 0.44  | 0.22  | 0.22  | 0.56  | 0.45   |
| S13.5/13.5/H3(s)     | 20                | 7             | 2309  | 1.03  | 0.07   | 0.96  | 0.17  | 0.79  | 0.87  | 0.50   |
| S13.5/13.5/H3(s/700) | 33                | 11            | 1906  | 0.82  | 0.07   | 0.75  | 0.29  | 0.46  | 0.75  | -  |
| S13.5/9/C3           | 45                | 14            | 602   | 0.25  | 0.01   | 0.24  | 0.13  | 0.11  | 0.24  | 0.33   |
| S12/12/C3            | 50                | 18            | 818   | 0.34  | 0.01   | 0.33  | 0.19  | 0.14  | 0.33  | 0.21   |
| S12/12/C3(s)         | 46                | 16            | 1372  | 0.72  | 0.25   | 0.47  | 0.26  | 0.21  | 0.52  | -  |
| S12/9/C3             | 43                | 13            | 1391  | 0.63  | 0.09   | 0.54  | 0.33  | 0.21  | 0.53  | -  |
| S9/9/C3              | 20                | 3             | 1938  | 1.00  | 0.13   | 0.87  | 0.00  | 0.87  | 0.70  | 0.51   |
| NS                   | -                 | -             | 1297  | 0.70  | 0.30   | 0.40  | 0.02  | 0.38  | 0.39  | 0.27   |

464 <sup>a</sup> Activation Yield =  $(m_{\text{nanoporous carbon}} / m_{\text{acid-char}}) \times 100$

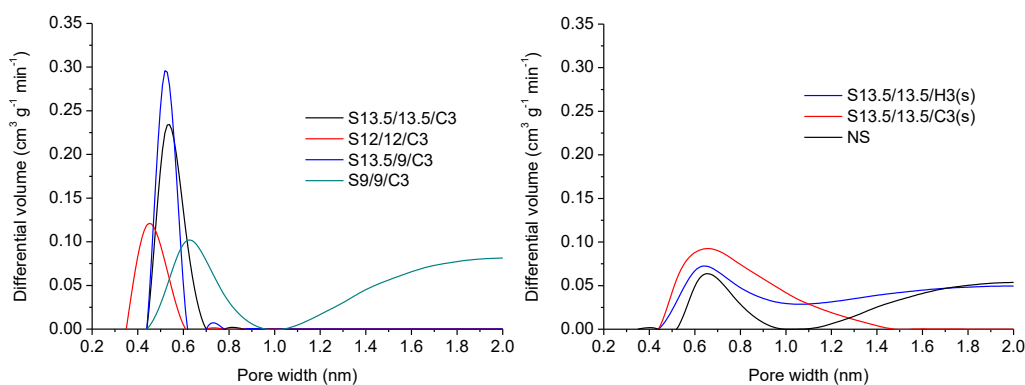
465 <sup>b</sup> Global Yield =  $(m_{\text{nanoporous carbon}} / m_{\text{sisal}}) \times 100$

466 <sup>c</sup> Evaluated at  $p/p^0 = 0.975$  in the  $\text{N}_2$  adsorption isotherms at  $-196 \text{ }^\circ\text{C}$

467 <sup>d</sup> Difference between  $V_{\text{total}}$  and  $V_{\alpha}^{\text{total}}$

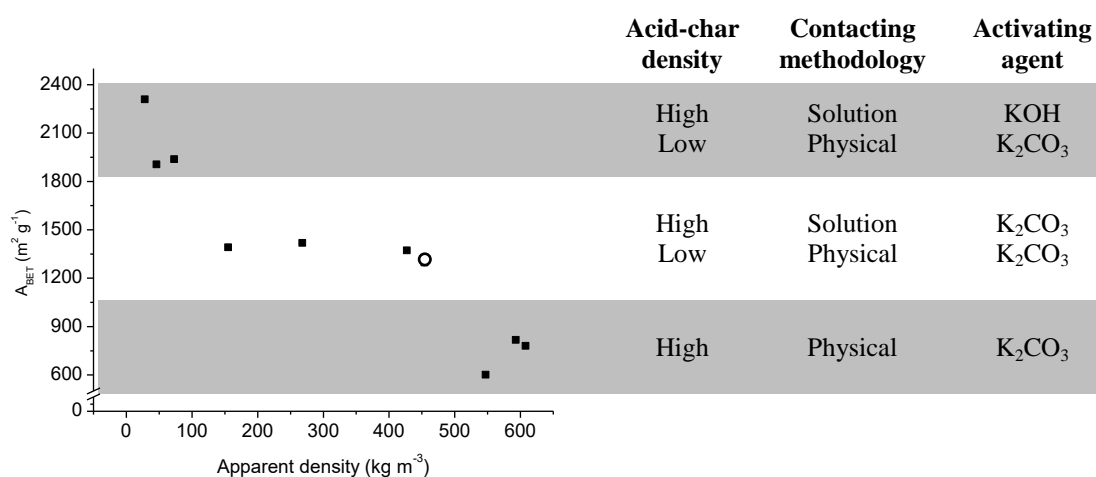
468

469



470 **Figure 5.** Micropore size distributions of the physically (left) and solution impregnated as well  
 471 as commercial sample (right) obtained by fitting the CO<sub>2</sub> adsorption isotherms at 0 °C to the  
 472 method described by Pinto *et al.* [30]. (A colour version of this figure can be viewed online).  
 473

474



475 **Figure 6.** Correlation between  $A_{\text{BET}}$  and apparent density of the synthesized nanoporous  
 476 carbons (squares) and the commercial sample (circle).

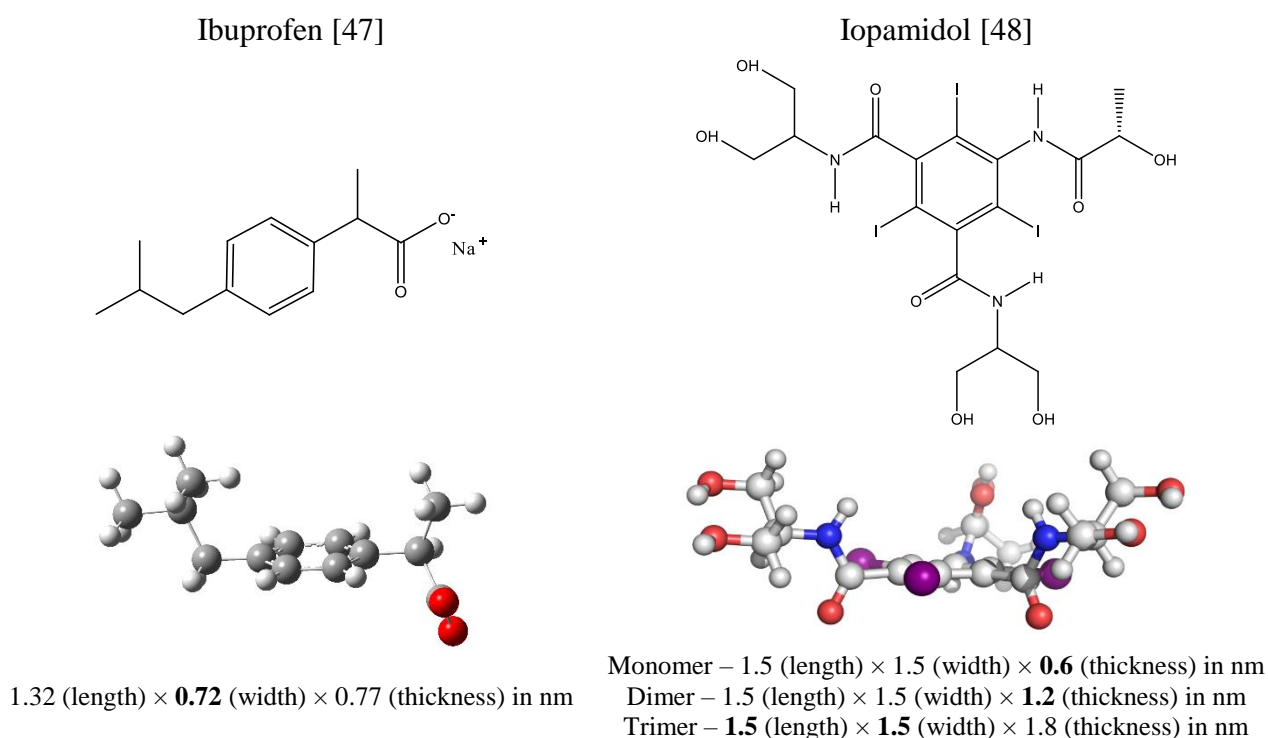
477

478 The activation of high density acid-chars with K<sub>2</sub>CO<sub>3</sub> by solution impregnation also  
 479 rendered materials with high surface areas ( $\approx 1400 \text{ m}^2 \text{ g}^{-1}$ ), a well-developed micro-  
 480 mesopore network, high activation and global yields (*ca.* 46-51 wt.% and 16-18 wt.%,  
 481 respectively) and apparent densities close to those of commercial samples. It must be  
 482 highlighted that such combination of porous features is not common by K<sub>2</sub>CO<sub>3</sub>  
 483 activation of low-ash content precursors.

484

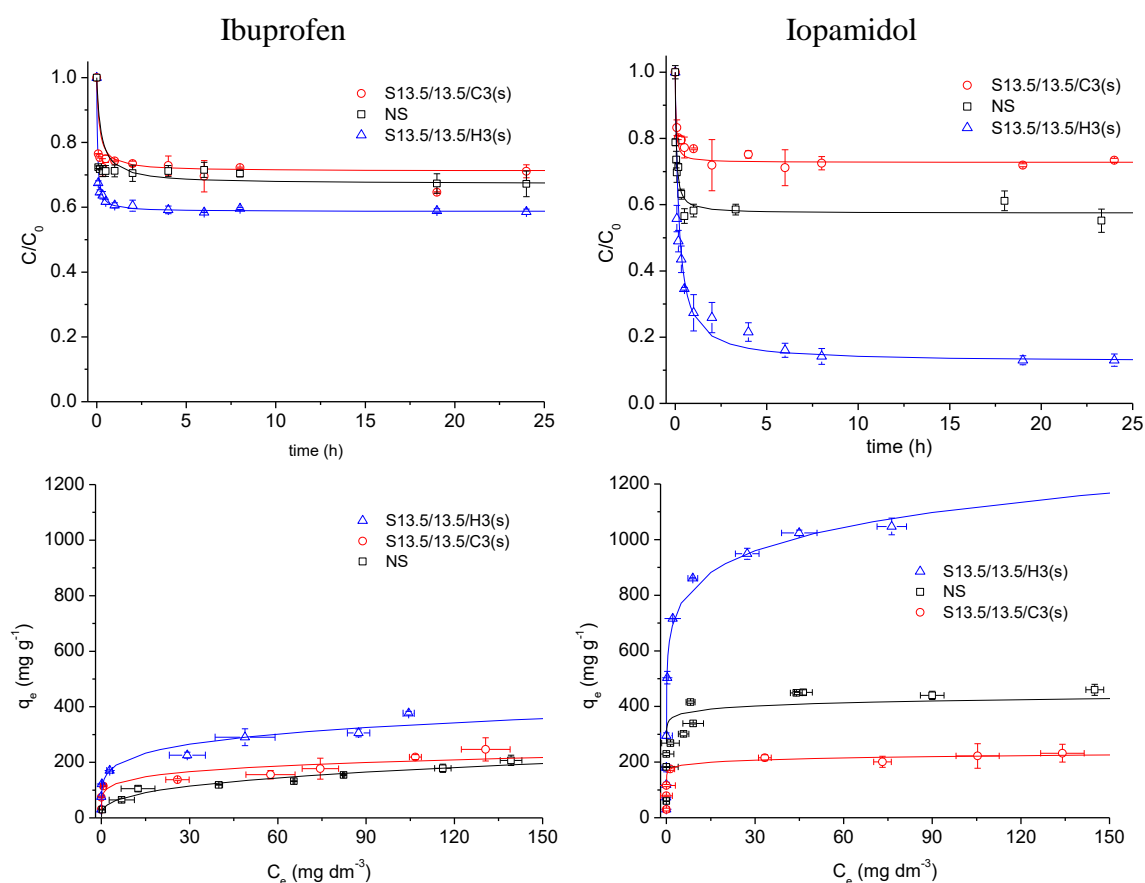
485 3.3 Ibuprofen and iopamidol adsorption onto selected nanoporous carbons

486 Based on screening assays, four nanoporous carbons were selected for the removal of  
487 ibuprofen and iopamidol (Figure 7), two active pharmaceutical ingredients commonly  
488 detected in wastewater effluents and drinking water. The removal efficiencies after 18 h  
489 of contact time are presented in Fig. S5. Samples S13.5/13.5/C3(s), S13.5/13.5/H3(s)  
490 and S9/9/C3 attained similar ibuprofen removal efficiencies in the range 40-45 %, as  
491 opposed to the low uptake of carbon S13.5/13.5/C3 (*ca.* 25 %). For iopamidol, the  
492 removal efficiencies of the selected carbons ranged between 10-74 %, following the  
493 sequence: S13.5/13.5/H(s) > S9/9/C3 > S13.5/13.5/C3(s) > S13.5/13.5/C3. The lower  
494 uptake of carbon S13.5/13.5/C3 for both compounds can be explained by its textural  
495 features (Table 2), therefore no additional studies were performed for this sample.



496 **Figure 7.** Structure and dimensions of ibuprofen sodium salt [47] and iopamidol species [48]  
497 (critical dimensions highlighted in bold).

498 Based on their distinct porous features, samples S13.5/13.5/C3(s) and S13.5/13.5/H3(s)  
 499 were selected for the kinetic and equilibrium assays, along with the commercial  
 500 activated carbon (NS). Data presented in Figure 8 show that sample S13.5/13.5/H3(s)  
 501 outperformed the commercial carbon (both in kinetic and equilibrium assays) for both  
 502 compounds, whereas the comparative balance for carbon S13.5/13.5/C3(s) vs the  
 503 commercial adsorbent was favourable only for ibuprofen. These results will be  
 504 discussed in terms of the combined effect of porous features and surface chemistry of  
 505 the materials.



506 **Figure 8.** Kinetic results (top) and adsorption isotherms (down) of ibuprofen (left) and iopamidol  
 507 (right) adsorption at 30 °C. Symbols correspond to the experimental data while lines represent the  
 508 fitting to the pseudo-second order kinetic model (top) and the fitting to the Freundlich equation  
 509 (bottom). Error bars are included. Experimental conditions of the kinetic assays 6 mg carbon/30  
 510 cm<sup>3</sup> of pharmaceutical solution with 180 mg dm<sup>-3</sup>. (A colour version of this figure can be viewed  
 511 online).

512 Kinetic data was fitted to the pseudo-second order kinetic equation, with coefficients of  
513 determination higher than 0.98 (Fig. 8). With the exception of the adsorption of  
514 iopamidol on sample S13.5/13.5/H3(s), all the systems reached the equilibrium in about  
515 3 h. According to the pseudo-second order kinetic parameters for ibuprofen adsorption  
516 (Table 3) the three carbons show global adsorption rates of the same order of  
517 magnitude, although slightly lower  $k_2$  values (fast rate) were obtained for the carbons  
518 containing mesopores (samples S13.5/13.5/C3(s) and NS), despite the similar uptakes.  
519 The initial adsorption rate is 4.5 or 6.5 times faster in sample S13.5/13.5/H3(s) than in  
520 S13.5/13.5/C3(s) and NS (respectively), pointing out the key role of the larger  
521 micropores. These results are in agreement with previous data reported in the literature  
522 for the adsorption of small pharmaceutical compounds (i.e. atenolol, caffeine, ibuprofen  
523 acid form) on activated carbons [45, 49, 50].

524 In the case of iopamidol, the highest global adsorption rate was also attained by sample  
525 S13.5/13.5/H3(s). The different iopamidol uptakes at kinetic equilibrium attained by the  
526 three adsorbents limits the comparison and analysis of their initial adsorption rates since  
527 this kinetic parameter depends on both the global adsorption rate and the uptake.

528 The adsorption rate of S13.5/13.5/C3(s) and NS for both pharmaceutical compounds is  
529 similar. Sample S13.5/13.5/H3(s) has the highest uptake for both pollutants, in mmol  
530 per gram the uptake of ibuprofen being almost twice than that of iopamidol. Compared  
531 to the other two samples, carbon S13.5/13.5/H3(s) has at least twice the volume of  
532 supermicropores, and a continuous micropore size distribution (Figure 5). This seems to  
533 favour both the adsorption rate and the uptake of ibuprofen and iopamidol. Similar  
534 results have been reported for the adsorption of paracetamol and iopamidol in sucrose-  
535 derived carbons in similar experimental conditions [13].

537 **Table 3.** Pseudo-second order ibuprofen and iopamidol adsorption parameters at 30 °C for  
 538 carbons S13.5/13.5/C3(s), S13.5/13.5/H3(s) and commercial sample (NS):  $k_2$  is the pseudo-  
 539 second order rate constant;  $h$  is the initial adsorption rate;  $t_{1/2}$  is the half-life time;  $q_{e,calc}$  and  
 540  $C_{e,calc}$  are respectively, the PhC uptake and that remaining in solution at equilibrium both  
 541 calculated by the pseudo-second order kinetic model.

| Sample           | $k_2$<br>( $\text{g mg}^{-1} \text{h}^{-1}$ ) | $R^2$ | $h$<br>( $\text{mg g}^{-1} \text{h}^{-1}$ ) | $t_{1/2}$<br>(h) | $q_{e,calc}$           |                                       | $C_{e,calc}$<br>( $\text{mg dm}^{-3}$ ) |
|------------------|---|-------|---|------------------|------------------------|---------------------------------------|---|
|                  |   |       |   |                  | ( $\text{mg g}^{-1}$ ) | ( $\text{mmol g}^{-1}$ ) <sup>a</sup> |   |
| <i>Ibuprofen</i> |   |       |   |                  |                        |                                       |   |
| S13.5/13.5/C3(s) | 0.020   | 0.984 | 1568  | 0.175            | 280                    | 1.365                                 | 124                                     |
| S13.5/13.5/H3(s) | 0.052   | 0.999 | 7127  | 0.052            | 372                    | 1.813                                 | 106                                     |
| NS               | 0.013   | 0.998 | 1095  | 0.270            | 296                    | 1.443                                 | 121                                     |
| <i>Iopamidol</i> |   |       |   |                  |                        |                                       |   |
| S13.5/13.5/C3(s) | 0.109   | 0.998 | 6513  | 0.037            | 245                    | 0.315                                 | 131                                     |
| S13.5/13.5/H3(s) | 0.007   | 0.999 | 4088  | 0.193            | 787                    | 1.013                                 | 23                                      |
| NS               | 0.099   | 0.991 | 14704                                       | 0.026            | 385                    | 0.495                                 | 77                                      |

542 <sup>a</sup> Calculated considering the molecular weight of ibuprofen anion and iopamidol monomers.

543 Confronting the micropore size distributions (Figure 5) with the critical dimensions of  
 544 the pollutants (smallest section of the most stable configuration computed in aqueous  
 545 solution, highlighted in bold in Figure 7), it can be concluded that ibuprofen molecule  
 546 (critical dimension - 0.72 nm) [47] can be easily adsorbed on the three carbons, while  
 547 iopamidol (critical dimensions of 0.6, 1.2 or 1.5 nm, for the monomer, dimer or trimer,  
 548 respectively) [48] presents diffusional constrains for most of them, with the exception of  
 549 sample S13.5/13.5/H3(s) due to its continuous micropore size distribution. It is  
 550 interesting to note that carbon S13.5/13.5/C3(s) presents the lowest iopamidol uptake;  
 551 this could be explained by the negligible contribution of micropores wider than 1.2 nm,  
 552 that would allow the adsorption of iopamidol monomers but not dimers and trimers.  
 553 Additionally, the mesoporosity of this carbon is not capable of accommodating the  
 554 bulky iopamidol aggregates (dimers, trimers or even bigger aggregates), due to the

555 average mesopore size (Fig. S6) and the above-mentioned pore-blocking effects (Fig.  
556 3(b)). As a result, iopamidol removal on carbon S13.5/13.5/C3(s) does not follow the  
557 expected correlation with  $V_{\alpha \text{ super}} + V_{\text{meso}}$  reported in the literature [13, 48]. It should also  
558 be pointed out that in the case of carbon S13.5/13.5/C3(s) the concentration of  
559 iopamidol remaining in solution at equilibrium is higher than  $100 \text{ mg dm}^{-3}$ ; according to  
560 molar conductivities measurements [48], this is indicative of the presence of iopamidol  
561 molecular aggregates that would not accommodate in the micropores of this sample  
562 (Fig. 5). Bearing this in mind, it can be inferred that the high iopamidol uptake on  
563 samples S13.5/13.5/H3(s) and NS is favoured due to the presence of wider micropores  
564 that allow to achieve lower equilibrium concentration in solution (*ca.* 23 and  $77 \text{ mg dm}^{-3}$ ,  
565 respectively) preventing the formation of molecular aggregates in solution.

566 The equilibrium adsorption isotherms presented in Figure 8 are characterized by an  
567 initial rise followed by a slight continuous increase or a plateau depending on the  
568 system. The experimental data were fitted to the non-linear forms of the Langmuir [32]  
569 and Freundlich [33] equations; the fitting parameters, the adjusted coefficients of  
570 determination and reduced chi-square values are presented in Table 4.

571 In the case of ibuprofen, the three carbons present similar F-type curves, with ibuprofen  
572 uptake of sample S13.5/13.5/H3(s) being twice as big as that of carbon NS in the range  
573 of assayed concentrations. This is an agreement with the total micropore volumes of the  
574 adsorbents. F-type isotherms are indicative of multilayer adsorption in the sample,  
575 which would allow higher adsorption capacities with increasing the ibuprofen  
576 concentration in solution [33].

577 For iopamidol all the carbons show a steep initial rise in the isotherm, characteristic of a  
578 high affinity between the adsorbate and adsorbent. As in the case of ibuprofen, sample

579 S13.5/13.5/H3(s) stands out with a remarkably high adsorption capacity whereas sample  
 580 S13.5/13.5/C3(s) attains half the adsorption capacity of the commercial carbon NS.  
 581 Comparing the isotherms obtained for both PhCs, it is clear that iopamidol has higher  
 582 affinity for tested adsorbents than ibuprofen.

583 Regarding equilibrium data (Table 4) the adjusted coefficients of determination ( $R^2_{Adj}$ )  
 584 and reduced chi-square values ( $\chi^2_{Red}$ ) indicate a good fitting to the Freundlich model for  
 585 all the systems. For the particular case of iopamidol adsorption on carbons  
 586 S13.5/13.5/H3(s) and S13.5/13.5/C3(s), the  $R^2_{Adj}$  and  $\chi^2_{Red}$  values for Langmuir and  
 587 Freundlich fittings are very close; this indicates that both models can describe the  
 588 experimental data.

589 **Table 4.** Fitting parameters to the Langmuir and Freundlich models and chi-square test analysis,  
 590  $\chi^2_{Reduced}$ . Langmuir parameters:  $q_m$  - monolayer adsorption capacity,  $K_L$  – Langmuir constant.  
 591 Freundlich parameters:  $K_F$  – Freundlich constant ( $\text{mg}^{1-1/n} (\text{dm}^3)^{1/n} \text{g}^{-1}$ ),  $n$  – Freundlich exponent.

| Sample           | Langmuir equation               |   |                          |                             | Freundlich equation |  |                          |                             |
|------------------|---------------------------------|---|--------------------------|-----------------------------|---------------------|--|--------------------------|-----------------------------|
|                  | $q_m$<br>( $\text{mg g}^{-1}$ ) | $K_L$<br>( $\text{dm}^3 \text{mg}^{-1}$ ) | $R^2_{Adj}$ <sup>a</sup> | $\chi^2_{Red}$ <sup>b</sup> | $1/n$               | $K_F$<br>( $\text{mg}^{1-1/n} (\text{dm}^3)^{1/n} \text{g}^{-3}$ ) | $R^2_{Adj}$ <sup>a</sup> | $\chi^2_{Red}$ <sup>b</sup> |
| <i>Ibuprofen</i> |                                 |   |                          |                             |                     |  |                          |                             |
| S13.5/13.5/C3(s) | 278                             | 0.032                                     | 0.358                    | 3300                        | 0.167               | 94.2   | <b>0.669</b>             | <b>1700</b>                 |
| S13.5/13.5/H3(s) | 309                             | 0.586                                     | 0.703                    | 4334                        | 0.186               | 140.9  | <b>0.878</b>             | <b>1785</b>                 |
| NS               | 195                             | 0.064                                     | 0.839                    | 546                         | 0.333               | 36.9   | <b>0.948</b>             | <b>175</b>                  |
| <i>Iopamidol</i> |                                 |   |                          |                             |                     |  |                          |                             |
| S13.5/13.5/C3(s) | 219                             | 3.042                                     | 0.386                    | 3481                        | 0.053               | 173  | <b>0.389</b>             | <b>3462</b>                 |
| S13.5/13.5/H3(s) | 965                             | 3.109                                     | 0.881                    | 19527                       | 0.122               | 634  | <b>0.902</b>             | <b>15972</b>                |
| NS               | 447                             | 0.758                                     | 0.368                    | 11023                       | 0.040               | 351  | <b>0.763</b>             | <b>4139</b>                 |

592 <sup>a</sup>  $R^2_{Adj}$  – Adjusted coefficient of determination accounts for the degrees of freedom (DOF)

593 <sup>b</sup>  $\chi^2_{Red}$  – Reduced chi-square obtained by dividing the residual sum of squares (RSS) by the  
 594 degrees of freedom (DOF)

595 It should be mentioned that the water solubilities of ibuprofen sodium salt (ca. 100 000  
 596  $\text{mg dm}^{-3}$ ) and iopamidol (ca. > 200 000  $\text{mg dm}^{-3}$ ) [47]) are much higher than the range

597 of concentrations used in this study. Thus, this parameter is not expected to affect the  
598 different adsorption trends in the adsorption of these compounds.

599 Adsorption capacities are also expressed in mmol of PhC per gram of carbon (Table 5),  
600 to facilitate data comparison due to the differences in the molecular weights of  
601 ibuprofen and iopamidol. Using these units, it can be observed that carbon  
602 S13.5/13.5/H3(s) presents similar uptake of ibuprofen and iopamidol, despite the lower  
603 dimension of the former. This has to be attributed to the anionic character of ibuprofen  
604 at neutral pH, which would favor the interactions with water while decreasing affinity  
605 for adsorption.

606 **Table 5.** Amount of pharmaceutical compounds adsorbed for an equilibrium  
607 concentration in solution ( $C_e$ ) of  $90 \text{ mg dm}^{-3}$ . Values calculated from the fitting of the  
608 equilibrium adsorption data to Freundlich equation.

| Sample           | $q_{90 \text{ mg dm}^{-3}}$ <b>ibuprofen</b> |                                       | $q_{90 \text{ mg dm}^{-3}}$ <b>lopamidol</b> |                                       |
|------------------|--|---------------------------------------|--|---------------------------------------|
|                  | ( $\text{mg g}^{-1}$ )                       | ( $\text{mmol g}^{-1}$ ) <sup>a</sup> | ( $\text{mg g}^{-1}$ )                       | ( $\text{mmol g}^{-1}$ ) <sup>a</sup> |
| S13.5/13.5/C3(s) | 200  | 0.975                                 | 220  | 0.283                                 |
| S13.5/13.5/H3(s) | 325  | 1.584                                 | 1097   | 1.412                                 |
| NS               | 165  | 0.804                                 | 420  | 0.540                                 |

609 <sup>a</sup> Calculated considering the molecular weight of ibuprofen anion and iopamidol monomers.

610 Ibuprofen uptake (in  $\text{mmol g}^{-1}$ ) of S13.5/13.5/C3(s) is 3-times larger than that of  
611 iopamidol, most certainly due to diffusional constrains in the monomodal micropore  
612 network of this carbon centered at around 0.6-0.7 nm, which only allows the adsorption  
613 of iopamidol monomers and ibuprofen ions. The low iopamidol adsorption capacity (in  
614  $\text{mmol g}^{-1}$ ) of S13.5/13.5/C3(s) compared to S13.5/13.5/H3(s) and carbon NS  
615 demonstrates that when dealing with the adsorption of bulky molecules, it is essential to  
616 characterize the mesopore network. In fact, the complex mesopore network of sample  
617 S13.5/13.5/C3(s) would hinder the adsorption of iopamidol species, due to the sieving  
618 effects in the ink-bottle shape mesopores.

619 The effect of surface chemistry in the adsorption process must also be considered,  
620 particularly considering the different ionic state of ibuprofen and iopamidol. At the  
621 conditions of herein reported adsorption studies (aqueous solutions at pH 5) the surface  
622 of carbon S13.5/13.5/C3(s) is slightly negatively charged and ibuprofen is an anion,  
623 thus the results seem to point out that  $\pi$ - $\pi$  interactions predominate over electrostatic  
624 ones. Similarly, iopamidol is a neutral molecule thus the role of electrostatic  
625 interactions can be disregarded. In the case of the commercial carbon, the surface is  
626 slightly positively charged ( $\text{pH}_{\text{PZC}}$  of 8.4) and it presents a larger fraction of micropores  
627 compared to carbon S13.5/13.5/C3(s). Its slightly lower ibuprofen adsorption capacity  
628 thus confirms the hypothesis of a higher contribution of  $\pi$ - $\pi$  interactions over  
629 electrostatic ones in the adsorption of ibuprofen.

#### 630 4. Conclusion

631 We herein propose a two-step method for the valorization of a low density biomass  
632 waste (sisal, *Agave sisalana*) through the synthesis of acid-chars with varied density and  
633 morphology. The oxygen-rich surface and acidic nature of the acid-chars contributes to  
634 increase their reactivity during the activation step, making them excellent precursors for  
635 the preparation of high density nanoporous carbons with tailored pore structure in the  
636 full micro-mesopore range. This approach rendered carbon materials with better porous  
637 development when compared to the chemical activation of the same biomass precursor  
638 by traditional methods [42, 43]. Furthermore, these adsorbents outperformed  
639 nanoporous carbons commercialized for water remediation purposes, in terms of  
640 adsorption capacity and rate of two pharmaceutical compounds (ibuprofen and  
641 iopamidol). Both the acid-chars and their corresponding activated carbons display  
642 interesting textural, morphological and surface properties that make them promising  
643 materials for other applications in the fields of energy storage, catalysis, and as

644 electrode materials or supports of (bulky) molecules. In this regard, so far acid-chars  
645 have proven to be effective supports for the immobilization molybdenum catalysts for  
646 solventless olefins epoxidation [51].

#### 647 **Acknowledgements**

648 This work was developed under the financial support of projects  
649 UID/MULTI/00612/2013 (CQB) and UID/ QUI/50006/2013 -  
650 POCI/01/0145/FERDER/007265 (REQUIMTE) from FCT/MEC through national funds  
651 and co-financed by FEDER, under the Partnership Agreement PT2020. ASM thanks  
652 FCT for a Post-doctoral grant SFRH/BPD/86693/2012. The authors thank Cordex for  
653 supply of the sisal residues, Salmon & Cia for the supply of carbon NS, and Hovione  
654 for the supply of iopamidol.

655

#### 656 **References**

- 657 [1] Roskill Report, The Economics of Activated Carbon. Roskill Information Services,  
658 Ltd., Clapham Road, London, 1998.
- 659 [2] H. Marsh, F. Rodríguez-Reinoso, Activated Carbon, Elsevier, Oxford, 2006.
- 660 [3] K. Schaeffer, Activated carbon 2013 market update or, the carbon convolution, in:  
661 Water Conditioning & Purification, 2013.
- 662 [4] O. Ioannidou, A. Zabaniotou, Agricultural residues as precursors for activated  
663 carbon production - A review, Renew. Sust. Energ. Rev., 11 (2007) 1966-2005.
- 664 [5] M.A. Yahya, Z. Al-Qodah, C.W.Z. Ngah, Agricultural bio-waste materials as  
665 potential sustainable precursors used for activated carbon production: A review, Renew.  
666 Sust. Energ. Rev., 46 (2015) 218-235.
- 667 [6] A. Jain, R. Balasubramanian, M.P. Srinivasan, Hydrothermal conversion of biomass  
668 waste to activated carbon with high porosity: A review, Chem. Eng. J., 283 (2016) 789-  
669 805.

- 670 [7] V.K. Gupta, A. Nayak, B. Bhushan, S. Agarwal, A Critical Analysis on the  
671 Efficiency of Activated Carbons from Low-Cost Precursors for Heavy Metals  
672 Remediation, *Crit. Rev. Environ. Sci. Technol.*, 45 (2015) 613-668.
- 673 [8] A.M. Abioye, F.N. Ani, Recent development in the production of activated carbon  
674 electrodes from agricultural waste biomass for supercapacitors: A review, *Renew. Sust.  
675 Energ. Rev.*, 52 (2015) 1282-1293.
- 676 [9] A.S. Mestre, A.P. Carvalho, Nanoporous carbons synthesis: an old story with  
677 exciting new chapters, in: T. Ghrib (Ed.) *Porosity*, IntechOpen, April 26th 2018. DOI:  
678 [dx.doi.org/10.5772/intechopen.72476](https://doi.org/10.5772/intechopen.72476)
- 679 [10] C. Falco, J.P. Marco-Lozar, D. Salinas-Torres, E. Morallón, D. Cazorla-Amorós,  
680 M.M. Titirici, D. Lozano-Castelló, Tailoring the porosity of chemically activated  
681 hydrothermal carbons: Influence of the precursor and hydrothermal carbonization  
682 temperature, *Carbon*, 62 (2013) 346-355.
- 683 [11] M. Sevilla, A.B. Fuertes, R. Mokaya, High density hydrogen storage in  
684 superactivated carbons from hydrothermally carbonized renewable organic materials,  
685 *Energ. Environ. Sci.*, 4 (2011) 1400-1410.
- 686 [12] A.J. Romero-Anaya, M. Ouzzine, M.A. Lillo-Ródenas, A. Linares-Solano,  
687 Spherical carbons: Synthesis, characterization and activation processes, *Carbon*, 68  
688 (2014) 296-307.
- 689 [13] A.S. Mestre, E. Tyszko, M.A. Andrade, M. Galhetas, C. Freire, A.P. Carvalho,  
690 Sustainable activated carbons prepared from a sucrose-derived hydrochar: remarkable  
691 adsorbents for pharmaceutical compounds, *RSC Adv.*, 5 (2015) 19696-19707.
- 692 [14] A.S. Mestre, C. Freire, J. Pires, A.P. Carvalho, M.L. Pinto, High performance  
693 microspherical activated carbons for methane storage and landfill gas or biogas upgrade,  
694 *J. Mater. Chem. A*, 2 (2014) 15337-15344.
- 695 [15] M. Nunes, I.M. Rocha, D.M. Fernandes, A.S. Mestre, C.N. Moura, A.P. Carvalho,  
696 M.F.R. Pereira, C. Freire, Sucrose-derived activated carbons: electron transfer  
697 properties and application as oxygen reduction electrocatalysts, *RSC Adv.*, 5 (2015)  
698 102919-102931.

- 699 [16] M.-M. Titirici, R.J. White, C. Falco, M. Sevilla, Black perspectives for a green  
700 future: hydrothermal carbons for environment protection and energy storage, *Energ.*  
701 *Environ. Sci.*, 5 (2012) 6796-6822.
- 702 [17] L. Wang, Y. Guo, Y. Zhu, Y. Li, Y. Qu, C. Rong, X. Ma, Z. Wang, A new route  
703 for preparation of hydrochars from rice husk, *Bioresource Technol.*, 101 (2010) 9807-  
704 9810.
- 705 [18] M. Andrade, J.B. Parra, M. Haro, A.S. Mestre, A.P. Carvalho, C.O. Ania,  
706 Characterization of the different fractions obtained from the pyrolysis of rope industry  
707 waste, *J. Anal. Appl. Pyrol.*, 95 (2012) 31-37.
- 708 [19] L. Wang, Y. Guo, B. Zou, C. Rong, X. Ma, Y. Qu, Y. Li, Z. Wang, High surface  
709 area porous carbons prepared from hydrochars by phosphoric acid activation,  
710 *Bioresource Technol.*, 102 (2011) 1947-1950.
- 711 [20] M. Jorda-Beneyto, D. Lozano-Castello, F. Suarez-Garcia, D. Cazorla-Amoros, A.  
712 Linares-Solano, Advanced activated carbon monoliths and activated carbons for  
713 hydrogen storage, *Micropor. Mesopor. Mater.*, 112 (2008) 235-242.
- 714 [21] AWWA Standard for Powdered Activated Carbon, in, American Water Works  
715 Association, Denver, Colorado, 1996.
- 716 [22] CEFIC, Test methods for activated carbon, in, Conseil Européen des Fédérations  
717 de l'Industrie Chimique (European Council of Chemical Manufacturers' Federation),  
718 1986.
- 719 [23] J.S. Noh, J.A. Schwarz, Estimation of the point of zero charge of simple oxides by  
720 mass titration, *J. Colloid Interf. Sci.*, 130 (1989) 157-164.
- 721 [24] M. Thommes, K. Kaneko, A.V. Neimark, J.P. Olivier, F. Rodriguez-Reinoso, J.  
722 Rouquerol, K.S.W. Sing, Physisorption of gases, with special reference to the  
723 evaluation of surface area and pore size distribution (IUPAC Technical Report), *Pure*  
724 *Appl. Chem.*, 87 (2015) 1051-1069.
- 725 [25] J. Rouquerol, P. Llewellyn, F. Rouquerol, Is the bet equation applicable to  
726 microporous adsorbents?, in: P.L. Llewellyn, F. Rodriguez-Reinoso, J. Rouquerol, N.  
727 Seaton (Eds.) *Studies in Surface Science and Catalysis*, Elsevier, 2007, pp. 49-56.

- 728 [26] ISO9277, Determination of Specific Surface Area of Solids by Gas Adsorption -  
729 BET Method, Second Ed., in, ISO, Switzerland, 2010.
- 730 [27] F. Rouquerol, J. Rouquerol, K. Sing, Adsorption by Powders and Porous Solids -  
731 Principles, Methodology and Applications, Academic Press, San Diego, 1999.
- 732 [28] F. Rodriguez-Reinoso, J.M. Martin-Martinez, C. Prado-Burguete, B. McEnaney, A  
733 standard adsorption isotherm for the characterization of activated carbons, *J. Phys.*  
734 *Chem.*, 91 (1987) 515-516.
- 735 [29] J. Jagiello, J.P. Olivier, 2D-NLDFT adsorption models for carbon slit-shaped pores  
736 with surface energetical heterogeneity and geometrical corrugation, *Carbon*, 55 (2013)  
737 70-80.
- 738 [30] M.L. Pinto, A.S. Mestre, A.P. Carvalho, J. Pires, Comparison of Methods to Obtain  
739 Micropore Size Distributions of Carbonaceous Materials from CO<sub>2</sub> Adsorption Based  
740 on the Dubinin-Radushkevich Isotherm, *Ind. Eng. Chem. Res.*, 49 (2010) 4726-4730.
- 741 [31] Y.-S. Ho, Review of second-order models for adsorption systems, *J. Hazard.*  
742 *Mater.*, 136 (2006) 681-689.
- 743 [32] I. Langmuir, The adsorption of gases on plane surfaces of glass, mica and  
744 platinum, *J. Am. Chem. Soc.*, 40 (1918) 1361-1403.
- 745 [33] H.M.F. Freundlich, Over the adsorption in solution, *J. Phys. Chem.*, 57 (1906) 385-  
746 470.
- 747 [34] T.J. Bandoz, C.O. Ania, Surface chemistry of activated carbons and its  
748 characterization, in: T.J. Bandoz (Ed.) *Activated Carbon Surfaces in Environmental*  
749 *Remediation*, Elsevier, New York, 2006, pp. 159-229.
- 750 [35] B. Ruiz, I. Cabrita, A.S. Mestre, J.B. Parra, J. Pires, A.P. Carvalho, C.O. Ania,  
751 Surface heterogeneity effects of activated carbons on the kinetics of paracetamol  
752 removal from aqueous solution, *Appl. Surf. Sci.*, 256 (2010) 5171-5175.
- 753 [36] S. Biniak, G. Szymanski, J. Siedlewski, A. Swiatkowski, The characterization of  
754 activated carbons with oxygen and nitrogen surface groups, *Carbon*, 35 (1997) 1799-  
755 1810.

756 [37] P.E. Fanning, M.A. Vannice, A DRIFTS study of the formation of surface groups  
757 on carbon by oxidation, *Carbon*, 31 (1993) 721-730.

758 [38] H. Yu, S. Niu, C. Lu, J. Li, Y. Yang, Sulfonated coal-based solid acid catalyst  
759 synthesis and esterification intensification under ultrasound irradiation, *Fuel*, 208 (2017)  
760 101-110.

761 [39] M.-M. Titirici, M. Antonietti, Chemistry and materials options of sustainable  
762 carbon materials made by hydrothermal carbonization, *Chem. Soc. Rev.*, 39 (2010) 103-  
763 116.

764 [40] International Center for Diffraction Data. Power Diffraction File Alphabetical  
765 Index; International Center for Diffraction Data, in, Swarthmore PA, 1988.

766 [41] M. Thommes, K.A. Cychosz, Physical adsorption characterization of nanoporous  
767 materials: progress and challenges, *Adsorption*, 20 (2014) 233-250.

768 [42] A.S. Mestre, A.S. Bexiga, M. Proença, M. Andrade, M.L. Pinto, I. Matos, I.M.  
769 Fonseca, A.P. Carvalho, Activated carbons from sisal waste by chemical activation with  
770  $K_2CO_3$ : Kinetics of paracetamol and ibuprofen removal from aqueous solution,  
771 *Bioresource Technol.*, 102 (2011) 8253-8260.

772 [43] M.A. Andrade, R.J. Carmona, A.S. Mestre, J. Matos, A.P. Carvalho, C.O. Ania,  
773 Visible light driven photooxidation of phenol on  $TiO_2/Cu$ -loaded carbon catalysts,  
774 *Carbon*, 76 (2014) 183-192.

775 [44] M.A. Andrade, A.S. Mestre, C.O. Ania, A.P. Carvalho (unpublished work) 2018.

776 [45] S.C.R. Marques, A.S. Mestre, M. Machuqueiro, A.Ž. Gotvajn, M. Marinšek, A.P.  
777 Carvalho, Apple tree branches derived activated carbons for the removal of  $\beta$ -blocker  
778 atenolol, *Chem. Eng. J.*, 345 (2018) 669-678.

779 [46] J. Wang, S. Kaskel, KOH activation of carbon-based materials for energy storage,  
780 *J. Mater. Chem.*, 22 (2012) 23710-23725.

781 [47] A.S. Mestre, R.A. Pires, I. Aroso, E.M. Fernandes, M.L. Pinto, R.L. Reis, M.A.  
782 Andrade, J. Pires, S.P. Silva, A.P. Carvalho, Activated carbons prepared from industrial  
783 pre-treated cork: Sustainable adsorbents for pharmaceutical compounds removal, *Chem.*  
784 *Eng. J.*, 253 (2014) 408-417.

- 785 [48] A.S. Mestre, M. Machuqueiro, M. Silva, R. Freire, I.M. Fonseca, M.S.C.S. Santos,  
786 M.J. Calhorda, A.P. Carvalho, Influence of activated carbons porous structure on  
787 iopamidol adsorption, *Carbon*, 77 (2014) 607-615.
- 788 [49] M. Galhetas, A.S. Mestre, M.L. Pinto, I. Gulyurtlu, H. Lopes, A.P. Carvalho, Chars  
789 from gasification of coal and pine activated with  $K_2CO_3$ : Acetaminophen and caffeine  
790 adsorption from aqueous solutions, *J. Colloid Interf. Sci.*, 433 (2014) 94-103.
- 791 [50] A.S. Mestre, J. Pires, J.M.F. Nogueira, A.P. Carvalho, Activated carbons for the  
792 adsorption of ibuprofen, *Carbon*, 45 (2007) 1979-1988.
- 793 [51] C. Petit, M.V. Silva, A.S. Mestre, C.O. Ania, P.D. Vaz, A.P. Carvalho, C.D.  
794 Nunes, Sisal derived acid-char as support of Mo(II) complex for solventless olefin  
795 epoxidation, *ChemistrySelect*, (2018) DOI: 10.1002/slct.201802055.
- 796